

Non-reciprocity of Vortex-limited Critical Current in Conventional Superconducting Micro-bridges

Dhaval Suri,^{1, a)} Akashdeep Kamra,² Thomas N. G. Meier,³ Matthias Kronseder,⁴ Wolfgang Belzig,⁵ Christian H. Back,^{3, 6, 7} and Christoph Strunk⁴

¹⁾Department of Physics, Technical University of Munich, Garching 85748, Germany

²⁾Condensed Matter Physics Center (IFIMAC) and Departamento de Física Teórica de la Materia Condensada, Universidad Autónoma de Madrid, E-28049 Madrid, Spain

³⁾Department of Physics, Technical University of Munich, Garching b. Munich, Germany

⁴⁾Department of Physics, University of Regensburg, Regensburg, Germany

⁵⁾Fachbereich Physik, Universität Konstanz, D-78457 Konstanz, Germany

⁶⁾Munich Center for Quantum Science and Technology (MCQST), D-80799 München, Germany

⁷⁾Centre for Quantum Engineering (ZQE), Technical University of Munich, Garching, Germany

Non-reciprocity in the critical current has been observed in a variety of superconducting systems and has been called the superconducting diode effect. The origin underlying the effect depends on the symmetry breaking mechanisms at play. We investigate superconducting micro bridges of NbN and also NbN/magnetic insulator (MI) hybrids. We observe a large diode efficiency of $\approx 30\%$ when an out-of-plane magnetic field as small as 25 mT is applied. In both NbN and NbN/MI hybrid, we find that the diode effect vanishes when the magnetic field is parallel to the sample plane. Our observations are consistent with the critical current being determined by the vortex surface barrier. Unequal barriers on the two edges of the superconductor strip result in the diode effect. Furthermore, the rectification is observed up to a temperature ~ 10 K, which makes the device potential for diode based applications over larger temperature range than before.

In the presence of symmetry breaking potentials, the magnitudes of critical currents of a superconductor (SC) are unequal for the two bias polarities^{1–8}. This phenomenon is called the superconducting diode effect (SDE) and may arise due to simultaneous breaking of time reversal symmetry (TRS) and inversion symmetry (IS). The effect has gained attention in recent times for its potential applications in non-dissipative electronics. Assuming the critical current of SC to be determined by the critical depairing mechanism, theoretical models for the SDE rely on out-of-plane Rashba spin-orbit coupling^{9–13}, valley-Zeeman interaction¹⁴ etc. for the IS breaking and an applied magnetic field for the TRS breaking. As a result, SDE in SC is related to emergence of a chiral superconducting order^{9–11,13}.

The field witnessed an upsurge of reports spanning a range of systems such as van der Waals material with noncentrosymmetric crystal potential – MoS₂¹⁵, synthetic super lattice of Nb/V/Ta⁴, planar Josephson junction arrays of Al on InAs^{6,16}, magnetic proximity coupled heterostructures of van der Waals materials¹⁷ etc. These studies of the SDE rely primarily on the combination of magnetic fields and spin-orbit coupling, giving rise to magnetochiral anisotropy^{4,6,18–22}. Furthermore, it has been reported that an out-of-plane magnetic field can cause the diode effect due to valley-Zeeman spin-orbit interaction in NbSe₂¹⁴ or the imbalance in valley occupation in the case of twisted tri-layer graphene¹⁹. A recent experimental report has demonstrated non-reciprocal critical current in superconductor films as well as their hybrid with magnetic insulator employing small to no magnetic fields²³. Via careful experiments, spin-orbit

coupling was ruled out as the origin of the SDE. Instead, IS breaking in those experiments is provided by the non-identical edges of the superconducting film.

While a majority of the theoretical work has focused on the critical depairing mechanism, the critical current in type II superconductors is often determined by the vortex surface barriers^{24–27}. The supercurrent tries to pull vortices nucleated on one edge towards the other side, where they can be annihilated. At low supercurrents, the Bean-Livingston surface barrier²⁸ is strong enough to prevent the vortices from entering the superconductor. However, at a large enough current, which becomes the critical current, the Lorentz force overcomes the surface barrier resulting in flux flow through the film and destruction of the superconducting state^{24,25}. In case of a thin film, the lowest surface barrier is typically offered by the side surfaces for out-of-plane vortices resulting in a critical current significantly lower than the critical depairing current. Considering this mechanism, unequal vortex barriers owing to asymmetric local defects on the two side surfaces have been predicted to result in the SDE²⁹.

In this article, we find SDE in NbN micro-bridges in out-of-plane magnetic field. Furthermore, to investigate the effects of an in-plane exchange field, we study NbN/YIG and find no diode effect with in-plane applied fields. Since our device geometry avoids fringe fields caused by YIG from entering NbN, the absence of diode effect provides a test of the fringe-field mechanism of SDE put forth by Hou and coworkers²³. We attribute our observations to the critical current being determined by the vortex flow. Our results confirm that the SDE is caused by unequal vortex barriers on the two side surfaces of the film^{27,29}.

Our experiments use SiO₂ (100 nm) on Si and epitaxial Y₃Fe₅O₁₂ (YIG) (100 nm) on gadolinium gallium garnet

^{a)}Electronic mail: d.suri@tum.de

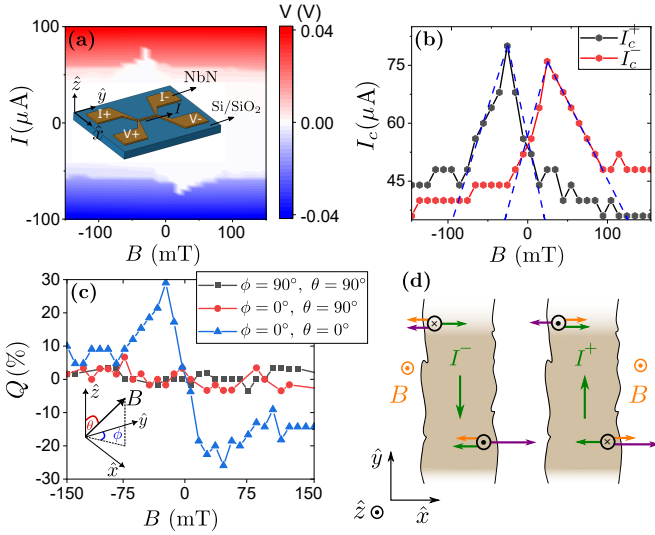


FIG. 1. (a) IV curves of the device at $T = 2$ K, as a function of magnetic field in the out-of-plane \hat{z} direction. Inset: schematic of the device used for experiments with the measurement configuration. (b) Critical current as a function of magnetic field extracted from fig. a, for positive and negative bias polarities. The precision of I_c is limited by step-size of the current sweep; this is $5 \mu\text{A}$ in our measurements. (c) Diode efficiency versus magnetic field, for three configurations of θ and ϕ as specified in the legend. $\theta = 90^\circ$ and $\theta = 0^\circ$ correspond to the configuration where the sample plane is parallel and perpendicular to the magnetic field, respectively. ϕ is the angle between I and B , when the sample plane is parallel to the magnetic field. $\phi = 0^\circ$ and $\phi = 90^\circ$ correspond to $I \parallel B$ and $I \perp B$, respectively. (d) Schematic depiction of the vortex instabilities at the two edges which determine the critical current. The arrows indicate forces on the vortices due to the transport current (green), the Meissner current (orange) generated by the applied magnetic field (assumed positive), and the vortex surface barrier (magenta). For transport current along $-\hat{y}$ (left panel), the critical current is determined by the left edge for $B \lesssim 20$ mT [corresponding to positive slope in (b)] and the right surface for $20 \text{ mT} \lesssim B \lesssim 100$ mT [negative slope in (b)]. For transport current along \hat{y} (right panel), the left edge determines the critical current at low B (> 0).

as substrates. A positive photo-resist was spun on the substrates, which was then patterned to micro devices via photo-lithography. The patterned sample was cleaned by soft sputtering Ar^+ ions in an ultra-high vacuum chamber, to eliminate any residual photo-resist and adsorbates. Further, NbN thin film was deposited using reactive DC magnetron sputtering at room temperature, at a base pressure $< 10^{-8}$ mbar. The sample was then dipped in acetone to lift off the film, resulting in micro devices. A standard 4-point measurement configuration using a DC current source and a nano-voltmeter was employed for the measurements [inset of fig. 1 (a)].

We first present the results of experiments on the 20 nm thick NbN device on SiO_2 demonstrating non-reciprocity of the critical current, I_c . The device is a micro-bridge of lateral dimensions $1 \mu\text{m} \times 4 \mu\text{m}$. The resistance versus temperature dependence of the device shows a broad transition to the superconducting state at $T_c = 7.5$ K [refer to fig. S3 in SI],

which corresponds to a Bardeen-Cooper-Schrieffer energy gap $2\Delta_0 = 4.05 k_B T_c$ equivalent to 1.3 meV, where k_B is the Boltzmann constant. The Ginzburg-Landau coherence length is estimated as³⁰ $\xi_{\text{GL}} = \sqrt{\hbar/\rho_N N_F e^2 \Delta_0} \approx 13.3$ nm, where $N_F \approx 10^{28}/(\text{m}^3 \text{eV})$ is the density of states in NbN at the Fermi level and e is the electronic charge. This places the Pearl length³¹ ($\lambda_P = 2\lambda_L^2/t$) at around $25 \mu\text{m}$ ($\gg w$) ensuring a spatially uniform current through the film. Here λ_L is the London penetration depth, derived using $\lambda_L = \sqrt{\hbar\rho_N/\pi\mu_0\Delta_0}$, where $l = 4 \mu\text{m}$, $w = 1 \mu\text{m}$, and $t = 20$ nm are length, width, and thickness of the bridge, respectively. ρ_N is the resistivity in the normal (N) state at low temperature when resistance is 400Ω , and μ_0 is the magnetic permeability in free space.

The current-voltage (IV) characteristics of the device as a function of magnetic field in the \hat{z} direction exhibits a decay of I_c with magnetic field up to ≈ 100 mT [fig. 1 (a)] and saturates for larger fields. We notice that the magnitude of maxima of critical currents ($\approx 80 \mu\text{A}$) in the two bias polarities are asymmetric about $B = 0$, indicating the emergence of non-reciprocity with respect to magnetic field. We plot the variation of I_c^+ and I_c^- as a function of magnetic field [fig. 1 (b)], and notice that $I_c^+ > I_c^-$, when $B < 0$ and vice versa when $B > 0$, demonstrating rectification. The figure of merit of the diode efficiency is defined by $Q = \frac{I_c^+ - I_c^-}{I_c^+ + I_c^-}$. The maximum efficiency of our device is ≈ 0.3 at $T = 2$ K and $B \approx \pm 25$ mT, illustrating a robust diode effect in the device. To investigate the underlying mechanism causing the diode effect in NbN, we study the variation of Q as a function of angle between the current and magnetic field directions. We find that the diode effect vanishes when the applied magnetic field is in the plane of the sample, irrespective of the in-plane angle (ϕ) [fig. 1 (c)]. The critical current as a function of out-of-plane magnetic field has been studied in NbN previously, however there was no report of non-reciprocity of the critical current³². In our experiments, three out of seven devices did not show any SDE despite fabrication under identical conditions, implying that the feature is highly sample dependent.

We interpret our findings assuming that the critical current is determined by the vortex flow^{24,25}. As discussed above, the critical current in our sample is the value at which the Lorentz force acting on out-of-plane vortices is able to overcome the net surface barrier and drive the vortices through the film. Following Ref. 27, we depict the forces on the relevant vortices near the left and the right edges in fig. 1 (d). Since the microstructure at the two edges are never identical^{27,29,33}, we assume the surface barrier at the right edge to be larger. Let us first consider the case of transport current along $-\hat{y}$ [fig. 1 (d) left panel]. At zero B , the critical current is determined by the weaker left edge surface barrier. As B (> 0) is increased, the Meissner screening currents caused by finite B exert additional forces on the vortices, thereby reinforcing the left surface barrier [fig. 1 (d) left panel] and enhancing the critical current. Since the Meissner response reinforces the left surface barrier while weakening the right surface barrier, at $B \approx 20$ mT, the vortex instability determining the critical current shifts to the right edge. Thus, the critical current decreases linearly

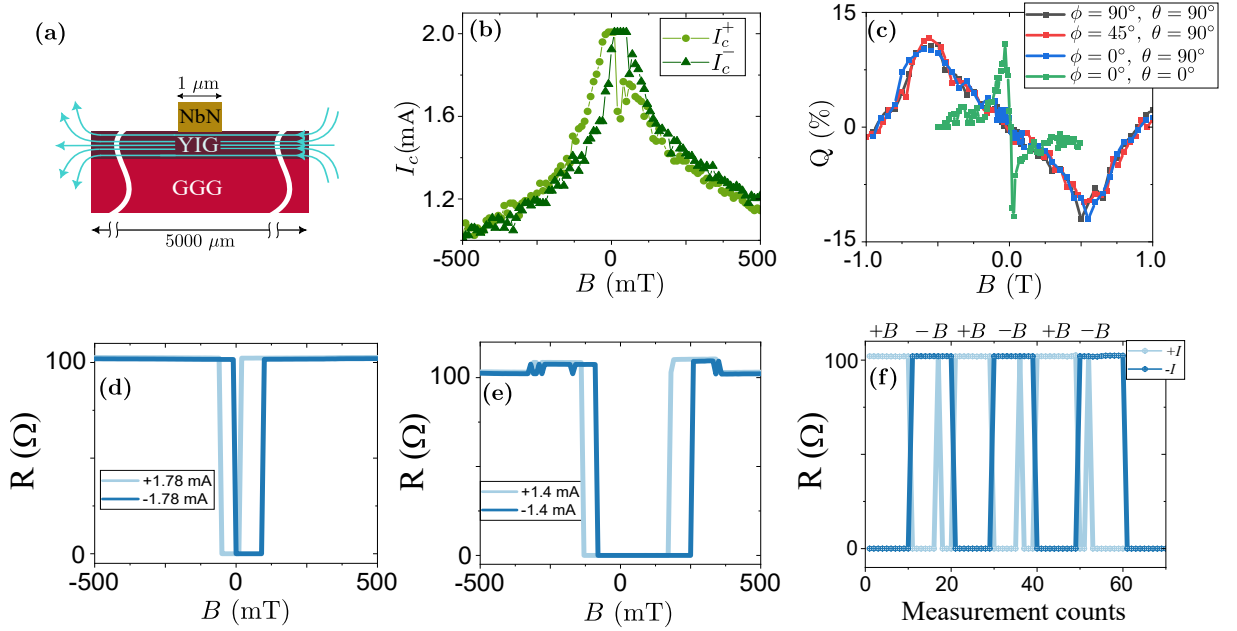


FIG. 2. (a) Schematic of the device cross-section. Lateral dimension of NbN ($\approx 1 \mu\text{m} \times 4 \mu\text{m}$) is orders of magnitude smaller than YIG/GGG ($\approx 5 \text{ mm} \times 5 \text{ mm}$); therefore the effect of fringe field on the micro-bridge is absent. The measurement geometry is the same as in fig. 1. YIG spreads over the whole substrate, making fringe field on the SC device negligible. (b) Critical current as a function of magnetic field for NbN/YIG device, for positive and negative bias polarities. (c) The diode efficiency versus magnetic field plotted at different angles between direction of magnetic field and current as specified in the legend. (d), (e) Resistance versus magnetic field in the out-of-plane direction for currents in both bias polarities at (d) 1.78 mA and (e) 1.4 mA. (f) Resistance switching between SC and normal states by changing magnetic field/bias polarity, showing robust diode effect at 7.3 K. The spikes in transition between SC and N states in the $+I$ curves are due to temperature fluctuations ($\approx 10 \text{ mK}$) which become visible close to T_c .

with $B^{24,27,29,34}$. On the other hand, for transport current along $+\hat{y}$ [fig. 1 (d) right panel], the left surface barrier is weakened by the Meissner currents leading to a linear decrease in the critical current. Combining these two cases, we see that the diode efficiency should increase linearly with B at low fields, as observed in fig. 1 (c). At $B \gtrsim 50 \text{ mT}$, the relevant vortex surface barrier has been lowered sufficiently such that bulk vortex pinning begins to determine the critical current. Therefore, the diode efficiency decreases, as the IS breaking caused by the surfaces starts to become irrelevant. The efficiency appears to saturate, instead of going to zero, possibly due to an internal and disorder-mediated IS breaking in the bulk pinning.

Complementing this qualitative analysis, we now extract the so-called maximum super-heating field of the Meissner state²⁴ B_s from our recorded critical current dependence on B [fig. 1 (b)]. This is the magnitude of B at which the linear decrease in I_c valid at low fields intercepts the magnetic field axis [blue dashed lines in fig. 1 (b)], when the whole curve is shifted along the B axis to make the critical current maximum occur at $B = 0$. We obtain 4 values for B_s (60 mT, 70 mT, 82 mT, 120 mT) from the four linear interpolations, each corresponding to the instability of a specific vortex (flux up or down) on a specific side (left or right). The difference in values of B_s probably arises due to different local superconducting properties near the two edges. The extracted values of B_s fit well with the theoretical

order-of-magnitude estimate of $\sim 30 \text{ mT}$ obtained using the expression:²³ $B_s = \phi_0 / (\sqrt{3}\pi\xi w)$, where ϕ_0 is the flux quantum.³⁶ The agreement between the B_s values obtained from our experiment and theory supports the validity of our assumed vortex mechanism of the critical current. Further confidence is gained from two observations: (i) variation of the critical current on a field scale of B_s , which is much smaller than the critical fields of NbN, and (ii) consistence between theoretical and experimental values of B_s in our work as well as the experiments by Hou and coworkers, who recorded an order of magnitude smaller B_s than ours due to their much wider samples.

With the aim of examining the helical superconducting state^{3,4,9,11,37} and the fringe field mechanisms of SDE, we study SC/magnetic insulator hybrids of NbN/YIG. Since our NbN film is grown on a much wider YIG film, our device design practically eliminates the effect of fringe fields on NbN [fig. 2 (a)]. Diode effect in SC/ferromagnet hybrids has been reported previously, where the ferromagnet is metallic^{38–40} and insulating⁴¹. We chose to study an SC/MI hybrid owing to its advantages for non-dissipative electronics, and to eliminate a parallel electron transport channel. In our NbN/YIG device, the critical current exhibits non-reciprocity with diode efficiency factor $\approx 13\%$ [fig. 2 (b)]. In the configuration where the magnetic field is nominally in the plane of the sample, we observe that the $Q(B)$ [fig. 2 (c)] is isotropic with respect to the direction between magnetic

field and current. The diode characteristics can be attributed to a possible misalignment of the sample with respect to the magnetic field, where the out-of-plane magnetic field is non-zero. Even a minor misalignment $\approx 3^\circ$ is sufficient to lead to the observed diode non-reciprocal behavior. Furthermore, isotropic behavior in the ϕ dependence corroborates this inference; any likely contribution from the Rashba spin-orbit coupling or magneto-chiral effects, would result in anisotropy in the in-plane field configuration^{6,10,42}. Thus, our experiments rule out any role of the spin-orbit coupling and associated helical superconducting states in causing the SDE in our samples. Since our samples eliminate the fringe field effects, we observe basically zero SDE in our SC/MI sample under the in-plane field configuration. This supports the fringe-field mechanism²³ of SDE in samples with equal width of SC and MI layers (V/EuS), where the fringe fields affect the SC. The SDE in our SC/MI sample is due to the same vortex mechanism as discussed above, and we obtain B_s of ~ 100 mT from our experimental data [fig. 2 (b)]. Thus, the MI plays no important role in the SDE observed here.

Further, the switching between SC and N states is illuminated by analyzing the horizontal line-cut profiles of the surface plots [fig. 2 (d-e)] of IV curve at different B [refer to fig. S1 (b) in SI]. The device exhibits $I_c = \pm 2$ mA at $B = 0$. We plot the resistance of the device versus B at fixed values of current $|I| < |I_c|$ [fig. 2 (d-e)]. We observe switching between SC and N states, in addition to maintaining the non-reciprocity with respect to the two bias polarities. The critical field B_c (field at which the device transitions from SC to normal state), increases with a decrease in the current at which the resistance is measured. Furthermore, we notice that B_c is asymmetric about $B = 0$. For instance, for a given bias polarity $+1.4$ mA [fig. 2 (e)], $B_c^+ = 180$ mT and $B_c^- = -120$ mT. These observations are consistent with the correlation between $B_c(T)$ and $I_c(T)$ of a superconductor. For each value of current, there exists a region of magnetic field where the device is superconducting in the positive bias and normal in the opposite, and vice versa. Keeping the magnetic field constant within the regime of non-reciprocity, we can observe the canonical diode effect [fig. 2 (f)] over multiple measurement cycles. The resistance of the device indicates switching from the SC state to the N state and vice versa by reversing the polarity of either the magnetic field or current bias. In the switching curve corresponding to $I+$ there are additional sporadic jumps to normal state, which primarily arise from vortex instabilities due to small temperature fluctuations. Over multiple measurement cycles we found that these jumps are random in nature, and absent at lower temperatures. We observe magneto-resistance switching up to 10 K [fig. S2 (b) in SI], enhancing the temperature regime in which the SC diode based experiments can be performed.

We have reported a robust superconducting diode in NbN and NbN/YIG micro devices, with diode efficiency of $\approx 30\%$. Absence of rectification in the in-plane field with magnetically saturated YIG film provides complimentary evidence to the report of Hou et al.,²³ that fringe fields are responsible for their observations on V/EuS. All our observations are consistent with the vortex surface barrier mechanism of the critical

current. In our best devices we find the resistance switching persistent up to 10 K which marks an advancement in the temperature range in which the diode based applications can be functional⁴³.

Acknowledgments— We thank J. S. Moodera, F. S. Bergeret and N. Paradiso for insightful discussions. AK acknowledges financial support from the Spanish Ministry for Science and Innovation – AEI Grant CEX2018-000805-M (through the “Maria de Maeztu” Programme for Units of Excellence in R&D). WB acknowledges funding by the Deutsche Forschungsgemeinschaft (DFG) through SFB 1432 (Project No. 425217212) and BE 3803/13 (Project No 465140728) as well as from the European Union’s Horizon 2020 FET Open programme SuperGate (Grant Number 964398). MK, CB and CS acknowledge funding by the Deutsche Forschungsgemeinschaft (German Research Foundation), Project-ID 314695032—SFB 1277 (Subprojects: A08 and B08).

- ¹Y. Tokura and N. Nagaosa, “Nonreciprocal responses from non-centrosymmetric quantum materials,” *Nat. Commun.* **9**, 3740 (2018).
- ²R. Wakatsuki and N. Nagaosa, “Nonreciprocal current in noncentrosymmetric rashba superconductors,” *Phys. Rev. Lett.* **121**, 026601 (2018).
- ³S. Hoshino, R. Wakatsuki, K. Hamamoto, and N. Nagaosa, “Nonreciprocal charge transport in two-dimensional noncentrosymmetric superconductors,” *Phys. Rev. B* **98**, 054510 (2018).
- ⁴F. Ando, Y. Miyasaka, T. Li, J. Ishizuka, T. Arakawa, Y. Shiota, T. Moriyama, Y. Yanase, and T. Ono, “Observation of superconducting diode effect,” *Nature* **584**, 373–376 (2020).
- ⁵T. Ideue and Y. Iwasa, “One-way supercurrent achieved in an electrically polar film,” *Nature* **584**, 349–350 (2020).
- ⁶C. Baumgartner, L. Fuchs, A. Costa, S. Reinhardt, S. Gronin, G. C. Gardner, T. Lindemann, M. J. Manfra, P. E. Faria Junior, D. Kochan, J. Fabian, N. Paradiso, and C. Strunk, “Supercurrent rectification and magnetochiral effects in symmetric josephson junctions,” *Nat. Nanotechnol.* **17**, 39–44 (2022).
- ⁷H. Wu, Y. Wang, Y. Xu, P. K. Sivakumar, C. Pasco, U. Filippozzi, S. S. P. Parkin, Y.-J. Zeng, T. McQueen, and M. N. Ali, “The field-free josephson diode in a van der waals heterostructure,” *Nature* **604**, 653–656 (2022).
- ⁸E. Strambini, M. Spies, N. Ligato, S. Ilić, M. Rouco, C. González-Orellana, M. Ilyn, C. Rogero, F. S. Bergeret, J. S. Moodera, P. Virtanen, T. T. Heikkilä, and F. Giazotto, “Superconducting spintronic tunnel diode,” *Nat. Commun.* **13**, 2431 (2022).
- ⁹N. F. Q. Yuan and L. Fu, “Supercurrent diode effect and finite-momentum superconductors,” *Proc. Natl. Acad. Sci.* **119**, e2119548119 (2022).
- ¹⁰S. Ilić and F. S. Bergeret, “Theory of the supercurrent diode effect in rashba superconductors with arbitrary disorder,” *Phys. Rev. Lett.* **128**, 177001 (2022).
- ¹¹A. Daido, Y. Ikeda, and Y. Yanase, “Intrinsic superconducting diode effect,” *Phys. Rev. Lett.* **128**, 037001 (2022).
- ¹²T. Karabassov, I. V. Bobkova, A. A. Golubov, and A. S. Vasenko, “Hybrid helical state and superconducting diode effect in s/f/ti heterostructures,” *arXiv: 2203.15608* (2022).
- ¹³J. J. He, Y. Tanaka, and N. Nagaosa, “A phenomenological theory of superconductor diodes,” *New J. Phys.* **24**, 053014 (2022).
- ¹⁴L. Bauriedl, C. Bäuml, L. Fuchs, C. Baumgartner, N. Paulik, J. M. Bauer, K.-Q. Lin, J. M. Lupton, T. Taniguchi, K. Watanabe, C. Strunk, and N. Paradiso, “Supercurrent diode effect and magnetochiral anisotropy in few-layer nbse₂,” *arXiv: 2110.15752* (2021).
- ¹⁵R. Wakatsuki, Y. Saito, S. Hoshino, Y. M. Itahashi, T. Ideue, M. Ezawa, Y. Iwasa, and N. Nagaosa, “Nonreciprocal charge transport in noncentrosymmetric superconductors,” *Sci. Adv.* **3**, e1602390 (2017).
- ¹⁶C. Baumgartner, L. Fuchs, A. Costa, J. Picó-Cortés, S. Reinhardt, S. Gronin, G. C. Gardner, T. Lindemann, M. J. Manfra, P. E. F. Junior, D. Kochan, J. Fabian, N. Paradiso, and C. Strunk, “Effect of

- rashba and dresselhaus spin-orbit coupling on supercurrent rectification and magnetochiral anisotropy of ballistic josephson junctions,” *J. Phys. Condens. Matter* **34**, 154005 (2022)
- ¹⁷J. Shin, S. Son, J. Yun, G. Park, K. Zhang, Y. J. Shin, J.-G. Park, and D. Kim, “Magnetic proximity-induced superconducting diode effect and infinite magnetoresistance in van der waals heterostructure,” arXiv: 2111.05627 (2021)
- ¹⁸B. Pal, A. Chakraborty, P. K. Sivakumar, M. Davydova, A. K. Gopi, A. K. Pandeya, J. A. Krieger, Y. Zhang, M. Date, S. Ju, N. Yuan, N. B. M. Schröter, L. Fu, and S. S. P. Parkin, “Josephson diode effect from cooper pair momentum in a topological semimetal,” arXiv: 2112.11285 (2021).
- ¹⁹J.-X. Lin, P. Siriviboon, H. D. Scammell, S. Liu, D. Rhodes, K. Watanabe, T. Taniguchi, J. Hone, M. S. Scheurer, and J. I. A. Li, “Zero-field superconducting diode effect in small-twist-angle trilayer graphene,” arXiv: 2112.07841 (2021)
- ²⁰K. Yasuda, H. Yasuda, T. Liang, R. Yoshimi, A. Tsukazaki, K. S. Takahashi, N. Nagaosa, M. Kawasaki, and Y. Tokura, “Nonreciprocal charge transport at topological insulator/superconductor interface,” *Nat. Commun.* **10**, 2734 (2019).
- ²¹Y. M. Itahashi, T. Ideue, Y. Saito, S. Shimizu, T. Ouchi, T. Nojima, and Y. Iwasa, “Nonreciprocal transport in gate-induced polar superconductor SrTiO_3 ,” *Sci. Adv.* **6**, eaay9120 (2020).
- ²²G. L. J. A. Rikken, J. Fölling, and P. Wyder, “Electrical magnetochiral anisotropy,” *Phys. Rev. Lett.* **87**, 236602 (2001).
- ²³Y. Hou, F. Nichele, H. Chi, A. Lodesani, Y. Wu, M. F. Ritter, D. Z. Haxell, M. Davydova, S. Ilić, F. S. Bergeret, A. Kamra, L. Fu, P. A. Lee, and J. S. Moodera, “Ubiquitous superconducting diode effect in superconductor thin films,” arXiv: 2205.09276 (2022).
- ²⁴V. V. Shmidt, “The critical current in superconducting films,” *Sov. Phys. JETP* **30**, 1137–1142 (1970).
- ²⁵V. V. Shmidt, “Critical currents in superconductors,” *Sov. Phys. Uspekhi* **13**, 408–409 (1970).
- ²⁶M. Rocci, D. Suri, A. Kamra, G. Vilela, Y. Takamura, N. M. Nemes, J. L. Martinez, M. G. Hernandez, and J. S. Moodera, “Large enhancement of critical current in superconducting devices by gate voltage,” *Nano Lett.* **21**, 216–221 (2021).
- ²⁷M. K. Hope, M. Amundsen, D. Suri, J. S. Moodera, and A. Kamra, “Interfacial control of vortex-limited critical current in type-II superconductor films,” *Phys. Rev. B* **104**, 184512 (2021).
- ²⁸C. P. Bean and J. D. Livingston, “Surface barrier in type-II superconductors,” *Phys. Rev. Letters* **12**, 14–16 (1964).
- ²⁹D. Y. Vodolazov and F. M. Peeters, “Superconducting rectifier based on the asymmetric surface barrier effect,” *Phys. Rev. B* **72**, 172508 (2005).
- ³⁰G. De Simoni, F. Paolucci, P. Solinas, E. Strambini, and F. Giazotto, “Metallic supercurrent field-effect transistor,” *Nature Nanotechnology* **13**, 802–805 (2018).
- ³¹J. Pearl, “Current distribution in superconducting films carrying quantized fluxoids,” *Appl. Phys. Lett.* **5**, 65–66 (1964).
- ³²K. Ilin, D. Henrich, Y. Luck, Y. Liang, M. Siegel, and D. Y. Vodolazov, “Critical current of nb, nbn, and tan thin-film bridges with and without geometrical nonuniformities in a magnetic field,” *Phys. Rev. B* **89**, 184511 (2014).
- ³³A. G. Sivakov, O. G. Turutanov, A. E. Kolinko, and A. S. Pokhila, “Spatial characterization of the edge barrier in wide superconducting films,” *Low Temp. Phys.* **44**, 226–232 (2018).
- ³⁴P. G. De Gennes, *Superconductivity of Metals and Alloys*, Advanced book classics (Perseus, Cambridge, MA, 1999).
- ³⁵G. M. Maksimova, “Mixed state and critical current in narrow semiconducting films,” *Phys. Solid State* **40**, 1607–1610 (1998).
- ³⁶The expression for B_s has been evaluated as $B_s = \phi_0 / (2\pi\xi w)$ by several authors^{24,27,35}. However, since it is only an order-of-magnitude estimate, this difference of $\sqrt{3}/2 \approx 0.9$ with respect to the expression employed in the main text is not important.
- ³⁷V. M. Edel’shtein, “Characteristics of the cooper pairing in two-dimensional noncentrosymmetric electron systems,” *Sov. Phys. JETP (English Translation)* **68**, 1244–1249 (1989).
- ³⁸G. Carapella, P. Sabatino, and G. Costabile, “Asymmetry, bistability, and vortex dynamics in a finite-geometry ferromagnet-superconductor bilayer structure,” *Phys. Rev. B* **81**, 054503 (2010).
- ³⁹A. Papon, K. Senapati, and Z. H. Barber, “Asymmetric critical current of niobium microbridges with ferromagnetic stripe,” *Appl. Phys. Lett.* **93**, 172507 (2008).
- ⁴⁰G. Carapella, V. Granata, F. Russo, and G. Costabile, “Bistable abrikosov vortex diode made of a py-nb ferromagnet-superconductor bilayer structure,” *Appl. Phys. Lett.* **94**, 242504 (2009).
- ⁴¹N. Touitou, P. Bernstein, J. F. Hamet, C. Simon, L. Méchin, J. P. Contour, and E. Jacquet, *Appl. Phys. Lett.* **85**, 1742–1744 (2004).
- ⁴²M. Davydova, S. Prembabu, and L. Fu, “Universal josephson diode effect,” *Sci. Adv.* **8**, eabo0309 (2022).
- ⁴³J. Lustikova, Y. Shiomi, N. Yokoi, N. Kabeya, N. Kimura, K. Ienaga, S. Kaneko, S. Okuma, S. Takahashi, and E. Saitoh, “Vortex rectenna powered by environmental fluctuations,” *Nat. Commun.* **9**, 4922 (2018).

**SUPPLEMENTARY INFORMATION FOR THE ARTICLE
NON-RECIPROcity OF VORTEX-LIMITED CRITICAL
CURRENT IN CONVENTIONAL SUPERCONDUCTING
MICRO-BRIDGES**

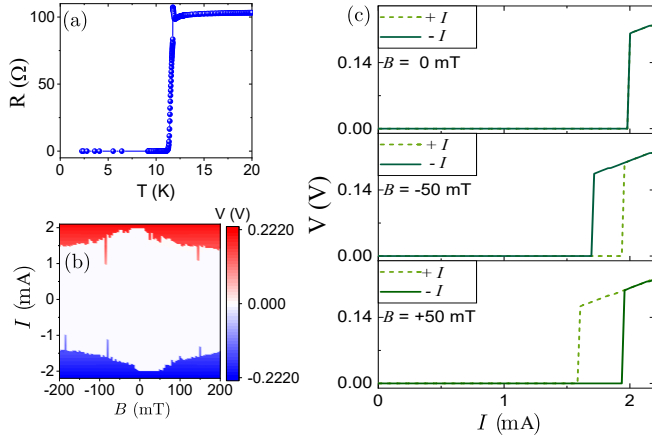


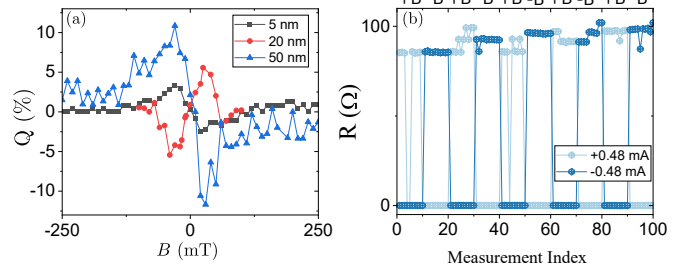
Fig. S1: (a) Resistance versus temperature of a 50 nm NbN/YIG device (b) IV curve of the device at different magnetic fields perpendicular to sample plane, at $T = 2$ K. (c) Absolute magnitude of the IV curves in positive and negative bias directions at $B = 0$, $B = -50$ mT and $B = +50$ mT, showing non-reciprocal critical current.

Fig. S1 (a) shows the resistance versus temperature of the NbN/YIG device with $T_c \approx 11$ K. The pre-transition peak close to T_c can be attributed to spatial inhomogeneities of the device as observed by earlier works on similar superconductors [Vaglio et al., Phys. Rev. B 47, 15302 (1993)]. In our device, we do not see any influence of the pre-transition peak on the diode effect. The resistance of the normal state observed in the IV curve is $\approx 97 \Omega$; whereas the resistance of the peak is larger, implying that the device transitions into stable resistive state in the IV curve. Fig. S1 (b) shows the IV curve of NbN/YIG device at different magnetic fields. We notice that the critical current is asymmetric with respect to magnetic field, $B = 0$. The sharp peaks in the IV curve (at ≈ -190 mT, -80 mT and $+150$ mT) are outliers; we do not find them consistently reproducible when the field sweep is repeated. Hence, they can be attributed to instabilities of the vortex distribution in the superconductor. To examine this carefully, we plot the IV curve at $B = 0$, $B = -50$ mT and $B = +50$ mT [fig. S1 (c)]. The critical current in the positive bias direction (I_{c+}) and negative bias direction (I_{c-}) are equal when $B = 0$. However, $I_{c+} > I_{c-}$ for $B < 0$ and vice versa for $B > 0$. This marks the SDE in NbN/YIG devices.

Fig. S2: (a) Diode efficiency factor for devices of varying thickness of NbN on YIG as shown in the legend, at $T = 2$ K. (b) Resistance of the device switching between

superconducting state and normal state either by reversing bias or field polarity at $T = 10$ K.

Fig. S2 (a) shows Q vs B for devices of different thicknesses of NbN on YIG, when the field is in the direction perpendicular to the sample. The nature of the diode effect



is different due to non-identical sample quality in each device. From this data, the dependence of magnitude of Q and the polarity on the thickness cannot be derived because the asymmetry in imperfections across the edges of the sample are not identical. Fig. S2 (b) shows the resistance switching between normal state to the superconducting state by changing either the bias direction or the direction of magnetic field $B = +50$ mT and $B = -50$ mT, at $T = 10$ K. The ability to switch the superconducting device at $T = 10$ K enhances the temperature regime over which diode based applications can be performed.

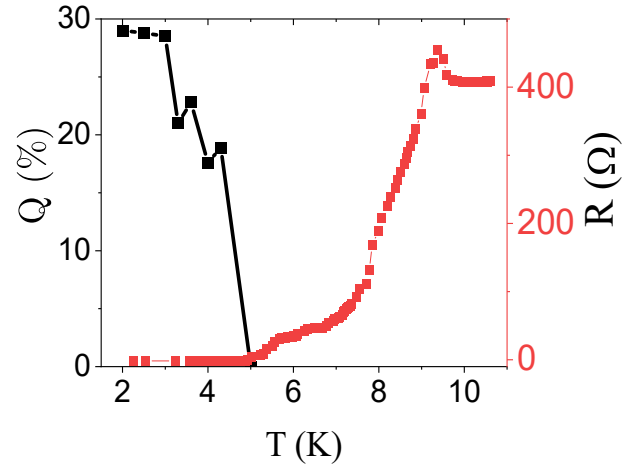


Fig. S3: Temperature dependence of the resistance of the device and the diode efficiency factor of a NbN/SiO₂ device.

Fig. S3 shows the temperature dependence of the resistance of the NbN device shown in the main text. The critical temperature (7.3 K) is slightly smaller than that of the film on YIG due to lower thickness of the film, implying a higher degree of disorder that is also reflected in a broader transition curve to the SC state. The temperature dependence of the diode efficiency factor increases with decrease in temperature and saturates at low temperatures. A generalized model for temperature dependence is of interest for further theoretical work.